Journal of Fluorescence
https://doi.org/10.1007/s10895-024-03801-x

RESEARCH

Novel Iminocoumarin-substituted Tetraphenylethylene-based Near-infrared Fluorescent Probe for Ratiometric Detection of F^- and H_2S

Yufeng Liu[1] · Jianing Yang[1] · Hongliang Liu[1] · Zhao Chen[1] · Gang Liu[1] · Shouzhi Pu[1,2]

Received: 29 March 2024 / Accepted: 6 June 2024

Abstract
An iminocoumarin and tetraphenylethylene compound that exhibits aggregation-induced emission (AIE) and a significant Stokes shift ($\Delta\lambda = 135$ nm) in THF was created via the Knoevenagel condensation method. **TPICBT** could also be used as a ratiometric near-infrared fluorescent probe for the naked color identification of F^- and H_2S. It showed a large red shift (> 90 nm), good selectivity, and anti-interference. Test strip detection and cell imaging had both been accomplished using the probe. In addition, the probe could conveniently detect H_2S produced during food spoilage without laboratory instruments.

Keywords AIE · Near-infrared fluorescent probe · Ratiometric detection · F^- · H_2S

Introduction

Fluorescent anion sensors have vital applications in food safety, biological monitoring, biomedicine, and other areas. Among the common anions, F^- performed a crucial role in industry, biology, and human daily life due to its smallest atomic radius, largest electronegativity, and strong Lewis basic properties [1]. For example, not only could it be used as an ingredient in toothpaste to treat osteoporosis, but it could also be used to purify uranium for nuclear weapons production. However, fluorine contamination was inevitably produced during the production processes, which disrupted many cell signaling processes and impeded the production of biological materials [2, 3]. Long-term consumption of high-fluorine water, food, and air by residents in high-fluorine areas would induce related diseases, such as fluorosis of the bones, cancer, neurological diseases, and so on. In addition, the degradation of some minerals and rocks on the slopes could also lead to an increase in fluoride ions in the aquatic environment, resulting in endemic fluorosis [4]. Therefore, it was crucial to create an effective and accurate procedure for F^- detection. In 1996, Kimura discovered that H_2S may be an endogenous neuromodulator present in the human brain [5, 6], which plays a significant role in the circulatory, respiratory, digestive, and central neurological systems [7–9]. H_2S was discovered in a variety of meals and was produced spontaneously by organic sulfur-rich foods such as meat, eggs, fruits, and vegetables [10]. The research showed that appropriate, low-concentration H_2S had a positive effect on food. H_2S, for instance, could increase the metabolic rate of the antioxidant enzymes, thus extending the time that food could be stored [11]. Nevertheless, H_2S in industrial wastes might harm mucous membranes, impair olfaction, and even kill people [12]. H_2S detection techniques have drawn a lot of discussion in recent years. The fluorescence detection approach was more effective at detecting H_2S than previous techniques due to its high sensitivity, non-invasive nature, ease of use, and other benefits [13–18]. As a result, it was essential to develop a new, accurate, and straightforward approach for H_2S analysis and detection in order to increase food security.

Intensity-varying fluorescent probes typically had a single emission peak and were prone to interference from ambient factors, instrument parameters, and light bleaching during the detection process. This could lead to inaccurate detections, so they were unsuitable for cell imaging

Yufeng Liu and Jianing Yang contributed equally to this work.

✉ Hongliang Liu
liuhongliang03@163.com

✉ Shouzhi Pu
pushouzhi@tsinghua.org.cn

[1] Jiangxi Key Laboratory of Organic Chemistry, Jiangxi Science and Technology Normal University, Nanchang 330013, PR China

[2] Institute of Carbon Neutral New Energy Research, Yuzhang Normal University, Nanchang 330031, China

Published online: 14 June 2024

Scheme 1 The mechanism of **TPICBT** identification of F^- and H_2S

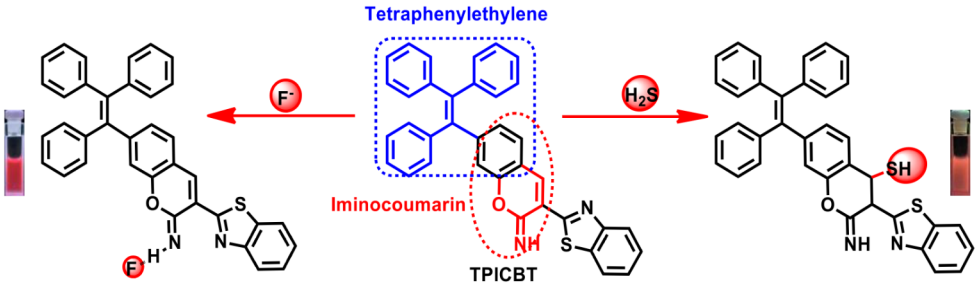

Scheme 2 Synthetic route of **TPICBT**

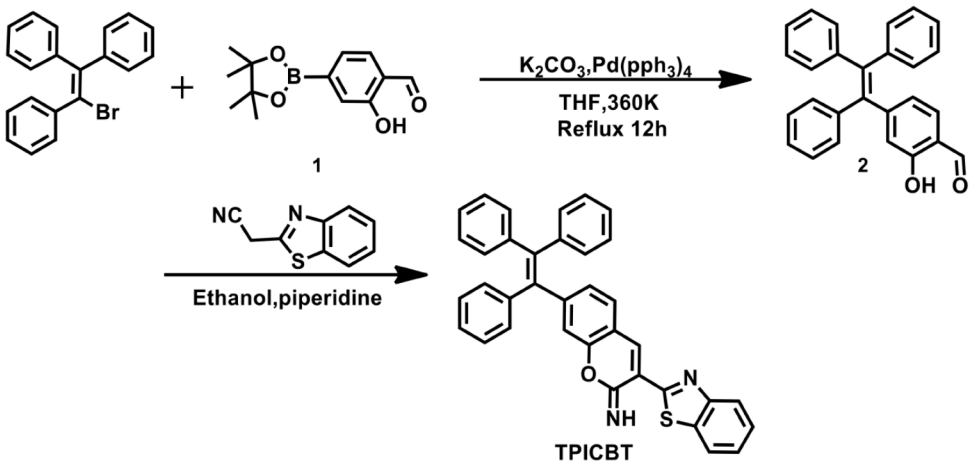

and food safety testing [19, 20]. In comparison to the switch model, the proportional sensing approach may provide an acceptable solution to the above problems because it could perform accurate analysis and testing by collecting the intensity ratio of the fluorescence probe's two emission peaks and its unique response. However, a substantial emission peak displacement was usually required to obtain good ratio measurement performance, as this could well divide the two simultaneous emission peaks and prevent luminescence spectra from overlapping [21–23]. Therefore, the presence of near-infrared (NIR) fluorescent probes was deemed more favorable because of their greater penetration, lower autofluorescence background, and less photodamage to biological materials [24–30]. Hence, the creation of ratiometric fluorescent probes possessing features of near-infrared emission has long been the center of our attention.

Benzothiazole and its derivatives play a significant role in fluorescent probes, drugs, functional molecules, dyes, sensors, and so on due to their strong rigid structure, robust optical support, and therapeutic efficacy. Additionally, benzothiazole derivatives also possessed an excellent quantum yield and an immense Stokes shift, so benzothiazole derivatives had been widely used by researchers to construct fluorescent probes [31–35].

F^- and H_2S were two important small molecules, but there were few probes that had a recognition response to both F^- and H_2S. Based on this, a new tetraphenylethylene and iminocoumarin-based naked-eye colorimetric fluorescent probe, **TPICBT**, was successfully synthesized by Knoevenagel condensation reaction in this work, which could realize dual recognition of F^- and H_2S (Scheme 1). **TPICBT** could detect F^- and H_2S in DMSO solution in a ratio-type, respectively, with a large red shift greater than 90 nm, and was already successfully utilized on test paper strips. In addition, the probe displayed strong cell-membrane penetration and may be used for identifying H_2S in active cells.

Experimental Section

General Methods

The agents were presented in the supporting information ESI.

Synthesis of TPICBT

The synthesis methods of **Compound 1** and **Compound 2** were shown in Schemes S1 and S2, and the relevant structural characterizations were listed in Figs. S1-S4. The synthesis route of **TPICBT** was shown in Scheme 2. After dissolving **Compound 2** (0.376 g, 1 mmol) and benzothiazol-2-acetonitrile (0.174 g, 1 mmol) in anhydrous ethanol, they were agitated for 0.5 h at room temperature in argon. Then piperidine was dropped and heated under an argon

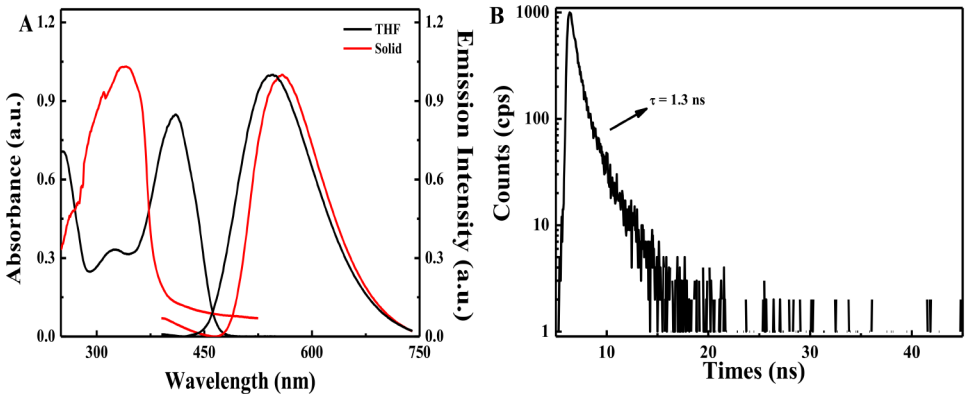

Fig. 1 (**A**) The absorption and fluorescence spectra of **TPICBT** in the free state (pure THF solution) and the concentrated state (solid state), and (**B**) fluorescence decay curve of **TPICBT** in the solid state

Table 1 Optical characterization of **TPICBT** in THF and solid state

Compound	Solution (THF)			Solid		
	λ_{max} (nm)[a]	λ_{em} (nm)[b]	τ (ns)[c]	λ_{max} (nm)[a]	λ_{em} (nm)[b]	τ (ns)[c]
TPICBT	323, 410	545	1.05 (f_w = 0%)	341	554	1.30

[a] Absorption wavelength

[b] The wavelength of the emission maximum

[c] The fluorescence lifetime

atmosphere for reflux for 5 h to obtain the crude product. Rinse with anhydrous ethanol to finally obtain compound **TPICBT** (0.315 g, 83.8%). ^{1}H NMR (500 MHz, DMSO-d_6) δ 9.06 (s, 1H), 8.65 (s, 1H), 8.13 (d, J = 5.0 Hz, 1H), 8.04 (d, J = 10.0 Hz, 1H), 7.60 (d, J = 5.0 Hz, 1H), 7.54 (t, J = 7.5 Hz, 1H), 7.44 (t, J = 7.5 Hz, 1H), 7.21–7.14 (m, 9H), 7.07–7.03 (m, 4H), 6.99 (d, J = 5.0 Hz, 2H), 6.85 (d, J = 10.0 Hz, 1H), 6.75 (s, 1H). ^{13}C NMR (126 MHz, $CDCl_3$) δ 156.4, 151.8, 147.1, 146.7, 142.5, 142.0, 142.0, 141.8, 138.4, 134.4, 132.5, 130.3, 130.2, 130.2, 127.0, 127.0, 126.8, 126.7, 126.6, 126.2, 125.9, 125.9, 122.1, 121.6, 118.1, 116.9, 116.6, 116.0, 110.6. ESI-MS (m/z): calcd for $C_{36}H_{24}N_2OS$: 533.1606 [**TPICBT** + H]$^+$, found: 533.1676 (Fig. S5-S7).

Results and Discussion

Optical Properties of Fluorescent Probe TPICBT

The photophysical properties of **TPICBT** in the free state (pure THF solution) and the concentrated state (solid state) were studied through ultraviolet absorption spectroscopy and fluorescence spectroscopy ($C = 2.0 \times 10^{-5}$ mol L^{-1}, λ_{ex} = 390 nm, slide = 5 nm / 5 nm), the fundamental spectral parameters shown in Fig. 1, and the basic spectral parameters were shown in Table 1. In pure THF solution, **TPICBT** had two absorption peaks at 323 nm ($\varepsilon = 1.66 \times 10^4$ L mol^{-1} cm^{-1}) and 410 nm ($\varepsilon = 4.23 \times 10^4$ L mol^{-1} cm^{-1}). The π-π* transition was responsible for the weak peak at 323 nm, while the formation of the strong absorption peak at 410 nm was primarily driven by the intramolecular charge transfer (ICT) of electrons between TPE and benzimidazole, which act as electron donors and acceptors, respectively [36]. In the solid state, **TPICBT**'s absorption peak was primarily at 341 nm ($\varepsilon = 5.16 \times 10^4$ L mol^{-1} cm^{-1}). Furthermore, as shown in Fig. 1A, when the λ_{ex} was 390 nm, the fluorescence spectrum of **TPICBT** in pure THF solution exhibited yellow-green fluorescence at 545 nm, and there was a large Stokes shift ($\Delta\lambda$ = 135 nm). It showed that **TPICBT** has low background interference and strong sample penetration, which could be better applied in cell imaging. In the solid state, the fluorescence emission peak of **TPICBT** displayed a bright yellow-green luminescence and was measured at 554 nm. Compared with **TPICBT** in pure THF solution, the solid emission peak showed a redshift of 9 nm and exhibited a larger Stokes shift ($\Delta\lambda$ = 213 nm). The variance between the two could be attributed to the variable fluorescent molecule accumulation patterns and fluorescent molecule interactions in the free-concentrated state [37]. In addition, the fluorescence decay curve in the substance state was also displayed in Fig. 1B, where a double exponential function value (τ) = 1.30 ns was calculated. Compared with the fluorescence lifetime index in the free state (τ) = 1.05 ns, this result further proved that **TPICBT** in the solid state could release energy in a fluorescent way due to molecular aggregation in solids and limited molecular motion [38, 39]. The comparison between the solid state and the free state showed that **TPICBT** had the properties of AIE.

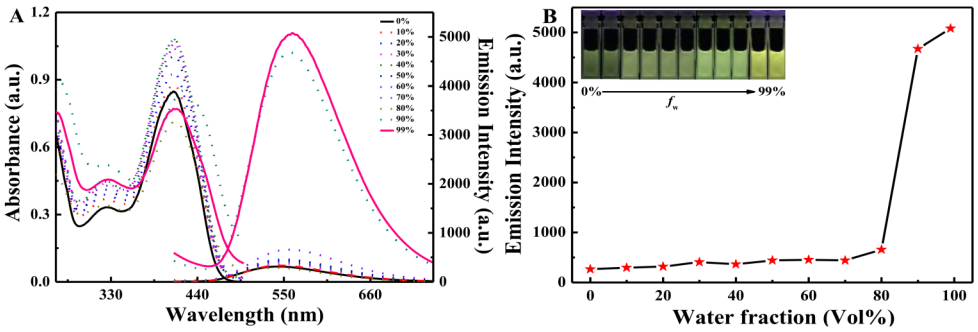

Fig. 2 (**A**) The absorption and fluorescence spectra of **TPICBT** (λ_{ex} = 390 nm) in THF/H_2O mixtures (C = 2.0 × 10^{-5} mol L^{-1}) with different f_w, and (**B**) the fluorescence intensities of **TPICBT** in different f_w at 560 nm (inset: **TPICBT** photos taken under 365 nm UV light)

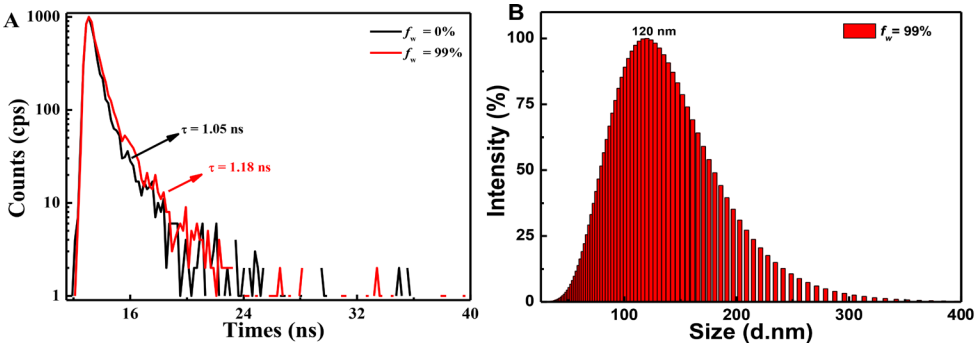

Fig. 3 (**A**) Fluorescence decay curve of **TPICBT** in THF/H_2O (f_w = 0, 99%, C = 2.0 × 10^{-5} mol L^{-1}) solution; (**B**) dynamic light scattering of **TPICBT** (f_w = 99%)

Aggregation-induced Emission (AIE) Properties of the Fluorescent Probe TPICBT

To further investigate the likely AIE characteristics of **TPICBT**, the UV-vis absorption and fluorescence spectra in the THF/H_2O mixture were studied at room temperature. Due to the formation of nanoaggregates and the Mie effect, the **TPICBT**'s absorption spectra, as displayed in Fig. 2A, had nearly identical absorption, and a noticeable level-off tail emerged in the long wavelength area [39]. In the fluorescence spectrum, it could be seen that **TPICBT** was incredibly low in pure THF, and the fluorescence yield of the quantum (Φ_f) was just 0.015. However, when the f_w gradually increases, the fluorescence intensity also gradually grows, and an abrupt increase in emission intensity was observed when the f_w was above 90%. And when the f_w was at 99%, the Φ_f of the solution was 0.058, which was about four times higher than that of pure THF. Additionally, when exposed to a 365 nm UV portable lamp, the fluorescence color of **TPICBT** could be found to change from yellow-green to bright yellow (inset: Fig. 2B). These occurrences might have resulted from **TPICBT**'s creation of nano-aggregates when the system's f_w was raised, which triggered the limitation of the intramolecular rotation (RIR) effect [40], thereby causing the high emission of the THF/H_2O mixture. The above results showed that **TPICBT** had a typical AIE effect.

Furthermore, since the fluorescence lifetime measurement was uncorrelated with the chromophore concentration and intensity of excitation, it could better illustrate the AIE characteristics of **TPICBT**. At a water percentage of 0% and 99%, the fluorescence lifetimes of **TPICBT** were 1.05 ns and 1.18 ns, respectively, as shown in Fig. 3A. Following that, Eqs. (1) and (2) were used to compute the average lifetime (τ) and quantum yield (Φ) in order to get the radiative rate constant (k_r) and non-radiative rate constant (k_{nr}). The calculated findings revealed that the k_r value grew from 0.014 ns^{-1} (f_w = 0%) to 0.049 ns^{-1} (f_w = 99%), whereas the k_{nr} value fell from 0.938 ns^{-1} to 0.797 ns^{-1}. The fluorescence enhancement was triggered by a rise in radiative rate constants and a fall in non-radiative rate constants. The results of f_w = 0% and f_w = 99% were consistent with the above conclusions. Further evidence from these findings pointed to the fact that constrained intramolecular rotation in aggregates impedes the non-radiative decay process and increases fluorescence.

$$\tau^{-1} = k_r + k_{nr} \quad (1)$$

$$k_r = \phi/\tau \quad (2)$$

Finally, we also carried out the DLS experiment in a mixed solution (f_w = 99%) to investigate the size of **TPICBT**. As shown in Fig. 3B, the average size of **TPICBT** nanoaggregates was 120 nm. This result indicated that **TPICBT** has the ability to self-assemble into nano-agglomerates in an aqueous solution, which strongly supports the material's AIE characteristics.

Selectivity and Anti-interference Ability of the Fluorescent Probe TPICBT

Firstly, in order to explore the selectivity of **TPICBT** for F^- and H_2S, the interaction between **TPICBT** and various anions was analyzed, including F^-, HS^-, CO_3^{2-}, SCN^-, HCO_3^-, HSO_3^-, SO_4^{2-}, Cl^-, NO_3^-, I^-, $H_2PO_4^-$, HSO_4^-, Br^-, NO_2^-, and $S_2O_3^{2-}$. As depicted in Fig. 4A, a peak at 388 nm was seen in the UV absorption spectrum of the probe **TPICBT**. However, until F^- was introduced, the initial absorption peak at 388 nm dropped, and a new peak appeared at 570 nm. Under sunlight, the color of visible light could be observed to range from yellow to bluish-purple (Fig. 4C). Besides, **TPICBT** would exhibit a novel absorption peak at 553 nm, and visible light would turn lavender instead of yellow in the presence of H_2S (Fig. 4C). But it could be found that the UV absorption wavelength of probe **TPICBT** combined with F^- was redshifted by 17 nm compared with H_2S. Moreover, the visible color difference between F^- and H_2S identified by **TPICBT** could be clearly distinguished with the naked eye. Therefore, this could be used as a standard to distinguish the two.

Then, as shown in Fig. 4B, when it was excited at 390 nm, the original fluorescence emission peak at 557 nm both disappeared after the addition of F^- and H_2S. Additionally, new emission peaks appeared at 657 nm and 653 nm in the near infrared, respectively, with a redshift of about 100 nm. And the fluorescence color changed from yellow to deep red and dark red when exposed to UV light (Fig. 4C). However, upon the addition of more ions, the **TPICBT** solution remained mostly unchanged (Fig. S8). These results showed that the probe **TPICBT** could achieve specific recognition of F^- and H_2S. In addition, we further assessed the anti-interference capabilities of **TPICBT**. As shown in Fig. S9A, when other ions were added to the solution for simultaneous existence with F^-, the fluorescence intensity did not change significantly. When other ions co-existed with H_2S, only the presence of F^- would enhance the fluorescence intensity as a whole, while the purity of other ions had no significant effect on the fluorescence intensity of Fig. S9B. The results showed that the probe had good anti-interference ability. Therefore, **TPICBT** was an outstanding near-infrared fluorescence probe for F^- and H_2S detection.

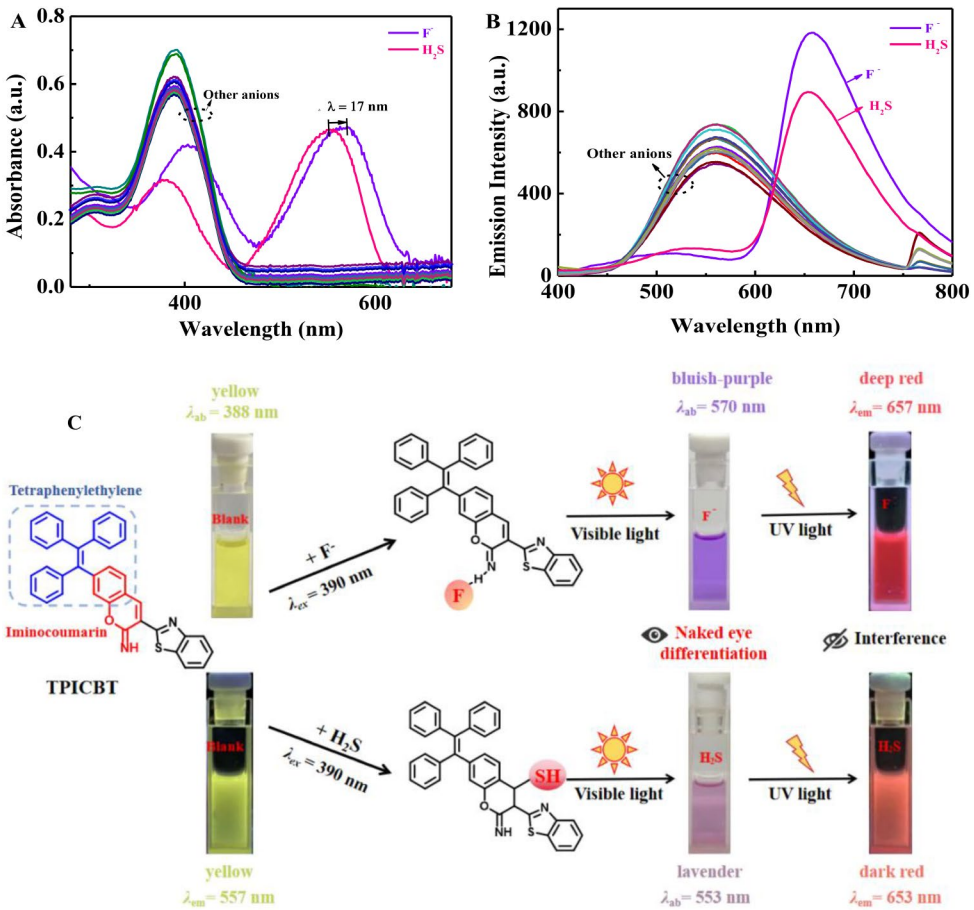

Fig. 4 (**A**) Absorption spectra; (**B**) fluorescence spectra of **TPICBT** ($C = 2.0 \times 10^{-5}$ mol L^{-1}) in the presence of contending anions; (C) comparison plot of **TPICBT** recognizing F^- and H_2S

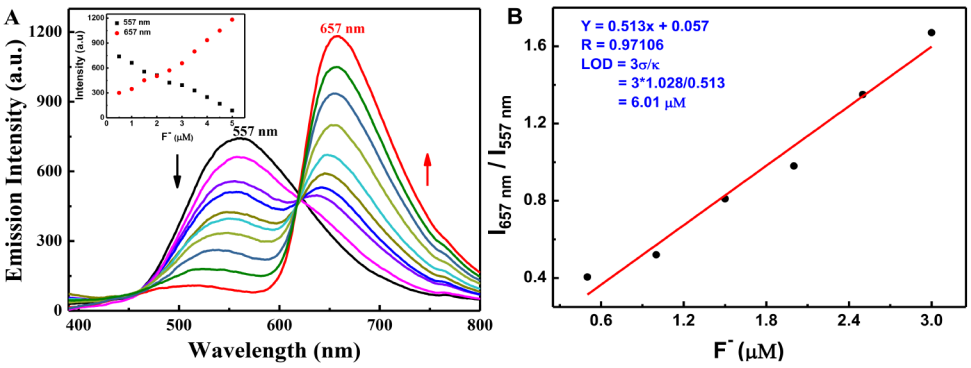

Fig. 5 (**A**) The fluorescence variation of **TPICBT** ($C = 2.0 \times 10^{-5}$ mol L^{-1}) induced by F^-, and (**B**) the linear relationship between the ratio of two fluorescence intensities (I_{657}/I_{557}) and F^- concentration in DMSO solution

Concentration Response and Detection Limit of Probe TPICBT on F^-

Moreover, to assess the dose-dependent response of **TPICBT**, the fluorescence and UV-vis response of **TPICBT** to F^- were measured by concentration titration at room temperature. When 0-2.6 eq. F^- were gradually added to the **TPICBT** solution, the absorption peak gradually decreased at 398 nm and increased at 562 nm (Fig. S10A). As shown in Fig. S10B, a wonderful linearity between absorbance ratios (A_{562}/A_{398}) and F^- concentration was acquired in the range of 1-4.5 μM ($Y = 0.23881*X - 0.15517$, $R = 0.99452$). At the same time, with the addition of F^-, the fluorescence peak at 657 nm gradually increased, while that at 557 nm gradually decreased (Fig. 5A). A clear isoborption point was observed at 620 nm, and the fluorescence quantum yield increased from 0.020 (**TPICBT**) to 0.042 (**TPICBT** + F^- complex), indicating that the probe **TPICBT** reacted with F^-. In addition, the radiation ratio (I_{657}/I_{557}), an important feature of the ratio response, increased from 0.41 to 13.6. In the range of 0.5-3.0 M, the emission ratio (I_{657}/I_{557}) versus the F^- concentration displayed an excellent linear correlation ($Y = 0.513*X + 0.057$, $R = 0.97106$) (Fig. 5B), indicating that the probe **TPICBT** may be able to accurately quantify F^-. Based on the reported mean value, the detection limit of **TPICBT** was computed to be 6.01 μM, which was far less than the World Health Organization's maximum pollutant level for F^- in drinking water (1.5 mg L^{-1}, about 80 mM) [41–43]. These findings demonstrated the potential of the **TPICBT** probe to be a ratio metric fluorescence probe for the visual identification of F^-, offering a quick and practical way to detect F^-.

Detection Mechanism of Fluorescent Probe TPICBT for F^-

Additional evidence of the probe **TPICBT**'s binding to F^- in DMSO-d_6 was provided by the ^{1}H NMR study (Fig. S12). The ^{1}H NMR contrast map showed that the chemical signal belonging to hydrogen on =NH, which was placed at 9.08 ppm, would gradually weaken and migrate to 9.05 ppm with the addition of F^-, but it did not fully disappear. The reason why the =NH proton did not deprotonate was caused by the extremely electronegative F^- engaging with it to form a hydrogen bond [44, 45]. Additionally, the maximum emission intensity of the [**TPICBT**] + [F^-] complex at 657 nm was seen when the mole fraction of [**TPICBT**]/([**TPICBT**] + [F^-]) was around 0.5, demonstrating a 1:1 stoichiometric ratio between **TPICBT** and F^- (Fig. S11). Finally, mass spectrometry was used to confirm the mechanism even further. The mass spectrum changes were depicted in Fig. 6, and the [**TPICBT** + H^+]$^+$ mass spectrum signal at m/z = 533.1676 increased to 552.1620 ([**TPICBT** + F^- + H^+]$^+$) (calcd. 552.1593) with the addition of F^-. These

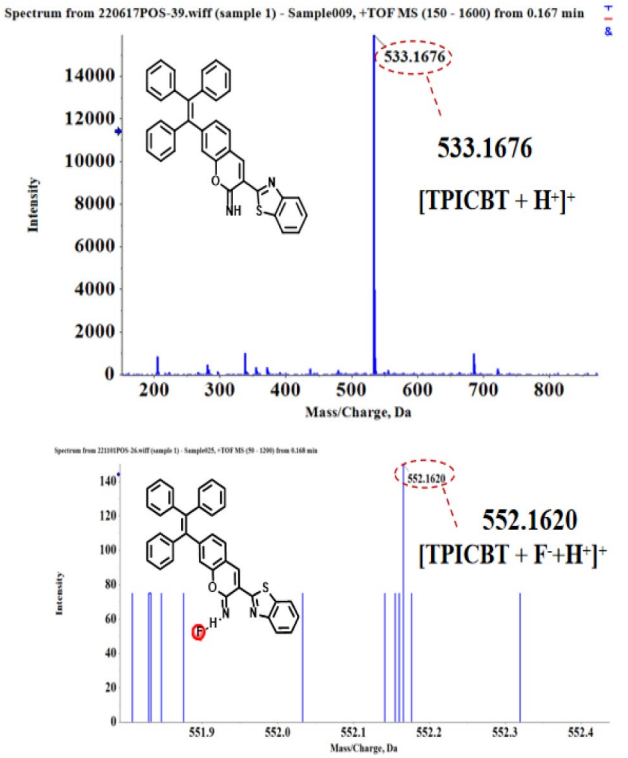

Fig. 6 Comparison of mass spectra of [**TPICBT** + H^+]$^+$ and [**TPICBT** + F^- + H^+]$^+$

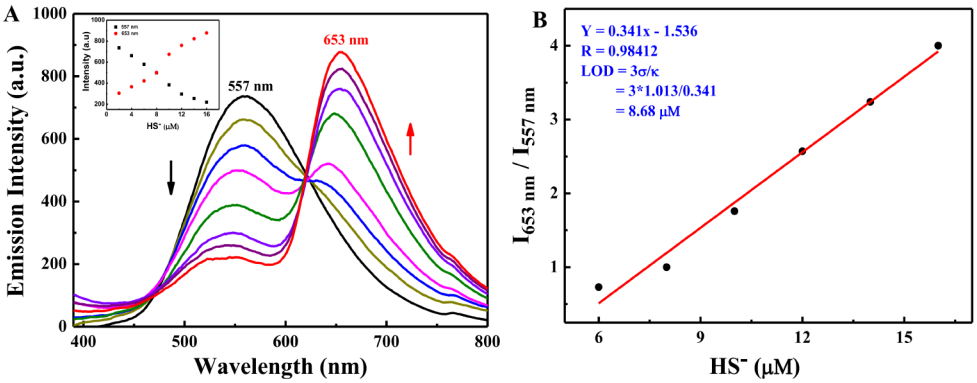

Fig. 7 (**A**) The fluorescence variation of **TPICBT** ($C = 2.0 \times 10^{-5}$ mol L^{-1}) induced by H_2S; (**B**) the linear relationship between the ratio of two fluorescence intensities (I_{653}/I_{557}) and H_2S concentration in DMSO solution

indicated that F bound to H in =NH and the deprotonation process did not occur.

Concentration Response and Detection Limit of Probe TPICBT on H_2S

According to previous literature, when an alkene C=C was coupled to an electron-withdrawing group, a Michael addition reaction involving nucleophilic mercaptans could directly start the reaction [46, 47]. Therefore, we conjectured that **TPICBT** could recognize H_2S by binding to C=C bonds. In order to test the recognition sensitivity of **TPICBT** to H_2S, concentration titration experiments were also performed. Upon gradually adding H_2S, a new peak at 548 nm and an isosbestic point at 450 nm appeared when the absorption intensity at 389 nm decreased. The absorption spectrum reached equilibrium following the addition of 8.0 eq. H_2S (Fig. S13A). It was discovered that the absorption intensity ratio (A_{548}/A_{389}) and the H_2S content had a linear connection in the 0–16 μM range (Y = 0.11785*X - 0.24479, $R = 0.98272$) (Fig. S13B). Additionally, Fig. 7A displays the **TPICBT**'s fluorescence spectra in reactions with various H_2S concentrations. The fluorescence emission peak of **TPICBT** at 557 nm progressively declines as H_2S is introduced, whereas it gradually increases at 653 nm, and an isorption point develops at 619 nm. Moreover, the emission ratio (I_{653}/I_{557}) against the H_2S concentration in the region of 6–15 μM displayed an excellent linear relationship (Y = 0.341*X - 1.536, $R = 0.98412$) (Fig. 7B). Using the equation LOD = 3σ/k, the detection limit of **TPICBT** toward H_2S was calculated to be 8.68 μM based on the slope of the curve and the standard deviation of the blank solution. The detection limit of the **TPICBT** probe was lower than the nationally permissible upper concentration of H_2S in the workplace of 10 ppm (15 mg/m^3) [48]. The above results showed that **TPICBT** was a sensitive H_2S detector.

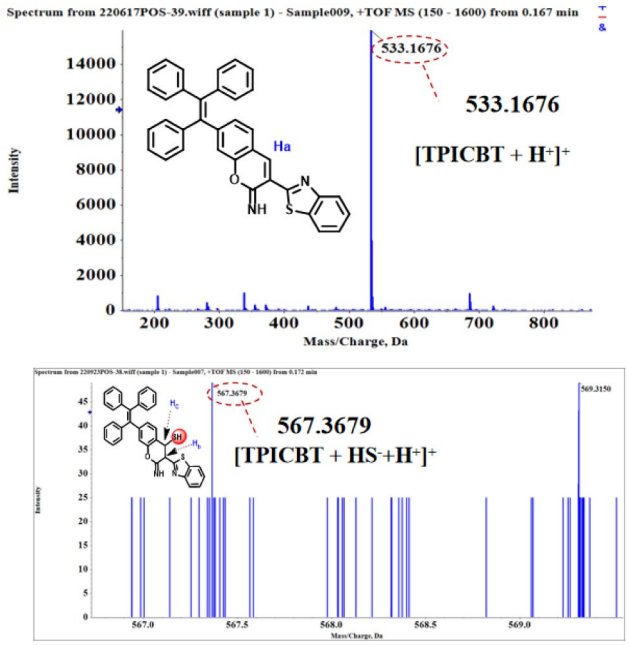

Fig. 8 Comparison of mass spectra of $[\mathbf{TPICBT}+H^+]^+$ and $[\mathbf{TPICBT}+HS^-+H^+]^+$

Detection Mechanism of Fluorescent Probe TPICBT for H_2S

In order to learn more about the chemical process between probe **TPICBT** and H_2S, ^{1}H NMR and mass spectra of the probe **TPICBT** were measured. Upon the addition of H_2S, the chemical shift at 8.11 ppm (H_a) disappeared due to H_2S attacking the C=C, while new signal peaks appeared at 4.38 ppm (C-H, H_b), 3.16 ppm (C-H, H_c), and 1.56 ppm (-SH) (Fig. S14). These results demonstrated that H_2S nucleophilic addition attacked the alkenyl group [49], which changed the fluorescence of the probe. Lastly, mass spectrometry was used to confirm the mechanism even further. The mass spectrum changes were depicted in Fig. 8, and the $[\mathbf{TPICBT}+H^+]^+$ mass spectrum signal at m/z = 533.1676 increased to 567.3679 ($[\mathbf{TPICBT}+HS^- + H^+]^+$) (calcd. 567.3679) with the addition of HS^-.

Table S1 listed some of the fluorescent probes that had been reported for the recognition of F^- and H_2S [50–59]. It was found that most of the fluorescent probes using TPE as a parent were almost off-on-type probes, rarely involving ratiometric-type probes. In comparison, the ratiometric probe was more accurate than the off-on probe, and these probes could not detect both F^- and H_2S simultaneously. In this work, **TPICBT** fluorescent probes could not only realize F^- and H_2S in ratiometric recognition but also the fluorescence emission peak at more than 650 nm. In the near-infrared region, it could be observed that the large redshifts (> 90 nm) and near-infrared probe could effectively reduce the interference of background, which was a good advantage in detection.

Practical Application of the Fluorescent Probe TPICBT

To evaluate the analytical application potential of **TPICBT** probes, filter paper was soaked in a DMSO solution containing **TPICBT**, dried in air, and deionized aqueous solutions of various ions were dropped on the test strip. As shown in Fig. 9, the test strip with other ions added did not change appreciably, but when F^- was added, the apparent color changed from light yellow to brilliant purple, as well as its fluorescent color switching from yellow to bright red. In addition, compared with the test strip for detecting F^-, the H_2S test strip's visible light color changed to dark purple, and the fluorescence color changed to dark red. The above phenomenon was similar to the fluorescence and ultraviolet test comparison diagram in Fig S8, and could be used as a proof to distinguish F^- and H_2S. According to these findings, the probe **TPICBT** could be utilized as a portable solid-state device for F^- and H_2S detection.

One of the primary volatile ingredients in the degradation of raw food was thought to be H_2S, a sulfur-containing bacterial metabolite. High H_2S residual concentrations from spoiled food could have negative health consequences for people [11, 60–63]. Therefore, the response experiment of the probe to the spoilage degree of raw meat was carried out. In this experiment, the color and fluorescence changes of the original meat sample strips were recorded. In the blank control group (Fig. S15), because the raw meat was stored at 0 ℃, it did not deteriorate and produce H_2S within 72 h, so the fluorescence and visible color of the test strip did not change within 72 h. According to Fig. 10, when raw beef was exposed to room temperature for 72 h, it partially decomposed and created H_2S, changing the color of the test paper from yellow to light purple and the fluorescence from bright yellow to light red. It showed that the test paper could sensitively detect H_2S gas emitted from rotten raw meat. The above results showed that **TPICBT** had a specific response to H_2S and might be applied as a method to evaluate raw meat freshness using simple dipstick assays.

Cell Imaging of the Fluorescent Probe TPICBT

To further evaluate whether **TPICBT** has practical application in organisms, we identified the cytotoxicity of **TPICBT** using the MTT method and observed whether fluorescence imaging of H_2S could be performed in HeLa cells. It was evident that after being exposed to **TPICBT** at doses of 0–20 μmol for 24 h, HeLa cells maintained at least 85% of their metabolic viability. In accordance with the findings, **TPICBT** exhibited high biocompatibility and low cytotoxicity (Fig. S16). Following that, the confocal laser scanning microscope (CLSM) was used to observe the ability of **TPICBT** to identify exogenous H_2S in HeLa cells ($\lambda_{ex} = 390$ nm). The uniform distribution of the green fluorescence signal in the cells (Fig. 11B_2) indicates that **TPICBT** successfully penetrated the cell membrane of HeLa cells. After the cells had been exposed to **TPICBT** (20 μM) and NaHS (50 μM) for 30 min, the cells thereafter displayed red fluorescence (Fig. 11C_2). The outcomes demonstrated the **TPICBT** probe's potential for imaging H_2S in living cells.

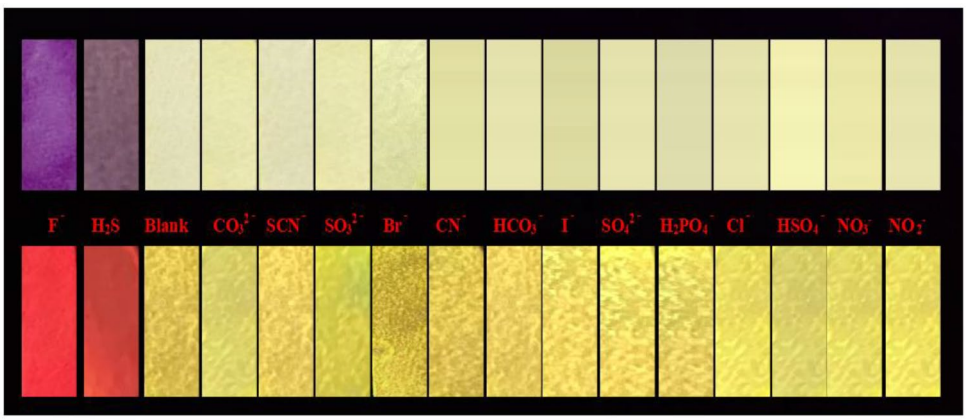

Fig. 9 Fluorescence and visible color change of different anions added to test strips, sunlight (up), and a 365 nm UV lamp (down)

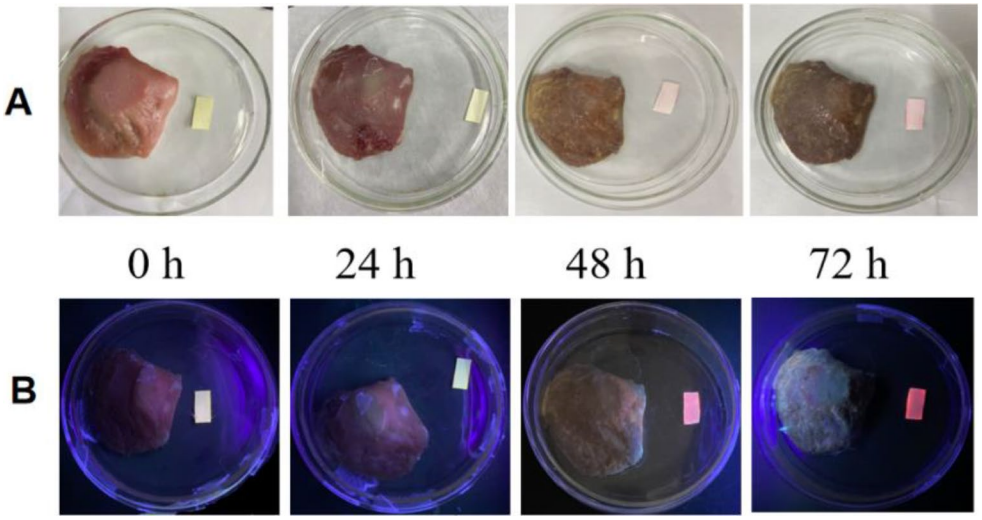

Fig. 10 At room temperature, photos of probe **TPICBT** detecting H_2S gas emitted from raw meat at different time periods: (**A**) sunlight; (**B**) a 365 nm UV lamp

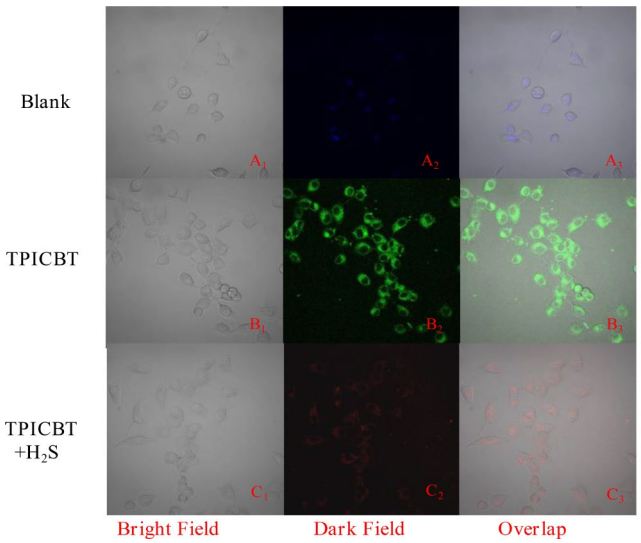

Fig. 11 Cell imaging of H_2S recognition by probe **TPICBT**, blank (A_1, A_2, A_3), **TPICBT** (B_1, B_2, B_3), and **TPICBT** + H_2S (C_1, C_2, C_3)

Conclusions

In summary, based on tetraphenylethylene and iminocoumarin, we have effectively designed and synthesized the probe **TPICBT** with high selectivity, a low detection limit, and a fast response. **TPICBT** had an obvious AIE effect with a relative redshift greater than 90 nm and could be used as a proportional near-infrared fluorescence probe for rapid detection of F^- and H_2S. In real life, the test strips made up of **TPICBT** probes could be used to quickly detect F^- and H_2S with the naked eye. In addition, **TPICBT** could sensitively detect the release of H_2S in raw meat, which could be used to detect the freshness of food. Moreover, because **TPICBT** has good cell permeability and is not hazardous to living things, it may be utilized as a fluorescent dye for cell fluorescence imaging. We think that this study's logical design approach could serve as an inspiration for the creation of more potent dual-responsive fluorescence probes for F^-/H_2S and other biomolecules.

Supplementary Information The online version contains supplementary material available at https://doi.org/10.1007/s10895-024-03801-x.

Author Contributions Yufeng Liu: Investigation, Data analysis, Writing. Jianing Yang: Investigation, Data analysis, Writing - Original Draft. Hongliang Liu: Validation, Writing - Review & Editing, Supervision. Zhao Chen: Review & Supervision. Gang Liu: Review & Supervision. Shouzhi Pu: Project administration, Funding acquisition.

Funding This research was financially supported by the National Natural Science Foundation of China (22263005), and the Jiangxi Science and Technology Normal University graduate student innovation special fund project in 2023 (YC2023-X01).

Data Availability No datasets were generated or analysed during the current study.

Declarations

Ethical Approval Ethics approval was not required for this research.

Competing Interests The authors declare no competing interests.

References

1. Chen XX, Leng TH, Wang CY, Shen YJ, Zhu WH (2017) A highly selective naked-eye and fluorescent probe for fluoride ion based on 1,8-naphalimide and benzothizazole. Dyes Pigm 141:299–305. https://doi.org/10.1016/j.dyepig.2017.02.008
2. Kai YM, Hu YH, Wang K, Zhi WB, Liang MM, Yang WG (2014) A highly selective colorimetric and ratiometric fluorescent chemodosimeter for detection of fluoride ions based on 1,8-naphthalimide derivatives, Spect. Acta Part A 118:239–243. https://doi.org/10.1016/j.saa.2013.08.100

3. Yu L, Li TT, Chen LG (2012) A fluorescent chemosensor for fluoride anions based on a hemicyanine dye. Res Chem Intermedlat 39:3525–3530. https://doi.org/10.1007/s11164-012-0859-4
4. Zhang B, Hong M, Zhang B, Zhang XL, Zhao YS (2007) Fluorine distribution in aquatic environment and its health effect in the Western Region of the Songnen Plain, Northeast China, Environ. Monit Assess 133:379–386. https://doi.org/10.1007/s10661-006-9592-z
5. Yu F, Han X (2014) Fluorescent probes for hydrogen sulfide detection and bioimaging. Chem Commun 50:12234–12249. https://doi.org/10.1039/c4cc03312d
6. Abe K, Kimura H (1996) The possible role of hydrogen sulfide as an endogenous neuromodulator. J Neurosci 16:1066–1071. https://doi.org/10.1523/JNEUROSCI.16-03-01066.1996
7. Zhao WM, Wang R (2002) H_2S-induced vasorelaxation and underlying cellular and molecular mechanisms. Am J Physiol-Heart C 283:474–480. https://doi.org/10.1152/ajpheart.00013.2002
8. Słowiński D et al (2021) Hymecromone naphthoquinone ethers as probes for hydrogen sulfide detection. Dyes Pigm 196:109765. https://doi.org/10.1016/j.dyepig.2021.109765
9. Kong F et al (2021) A double-locked probe for the detection of hydrogen sulfide in a viscous system. Chem Commun 54:6604–6607. https://doi.org/10.1039/d1cc01819a
10. Li SP, Zhang H (2014) Hydrogen sulfide alleviates postharvest senescence of broccoli by modulating antioxidant defense and senescence-related gene expression. J Agric Food Chem 62:1119–1129. https://doi.org/10.1021/jf4047122
11. Li D, Luo Z (2017) Effects of hydrogen sulfide on yellowing and energy metabolism in broccoli. Postharvest Biol Tec 129:136–142. https://doi.org/10.1016/j.postharvbio.2017.03.017
12. Keshtkar S, Rashidi A, Kooti M, Askarieh M, Pourhashem S, Ghasemy E, Izadi N (2018) A novel highly sensitive and selective H_2S gas sensor at low temperatures based on SnO_2 quantum dots-C_{60} nanohybrid: experimental and theory study. Talanta 188:531–539. https://doi.org/10.1016/j.talanta.2018.05.099
13. Yang B, Xu J, Zhu HL (2019) Recent progress in the small-molecule fluorescent probes for the detection of sulfur dioxide derivatives (HSO_3^2 /SO_3^2). Free Radical Biol Med 145:42–60. https://doi.org/10.1016/j.freeradbiomed.2019.09.007
14. Tang YF, Huang Y, Lu LX, Wang C, Sun TM, Zhu JL, Zhu GH, Pan JY, Jin YL, Liu AL, Wang M (2018) Synthesis of a new pyrene-devived fluorescent probe for the detection of Zn^{2+}. Tetrahedron Lett 59:3916–3922. https://doi.org/10.1016/j.tetlet.2018.09.038
15. Shi XR, Yin CX, Wen Y, Huo FJ (2019) A dual-sites fluorescent probe based on symmetric structure of naphthalimide derivative to detect H_2S. Dyes Pigm 165:38–43. https://doi.org/10.1016/j.dyepig.2019.02.014
16. Tang YF, Huang Y, Chen YH, Lu LX, Wang C, Sun TM, Wang M, Zhu GH, Yang Y, Zhang L, Zhu JL (2019) A coumarin derivative as a turn-on fluorescence probe toward Cd^{2+} in live cells, Spect. Acta Part A 218:359–365. https://doi.org/10.1016/j.saa.2019.03.104
17. Zhang H, Xu LZ, Chen WQ, Huang J, Huang CS, Sheng JR, Song XZ (2018) A lysosome targetable fluorescent probe for simultaneously sensing Cys/Hcy, GSH, and H_2S from different signal patterns. ACS Sens 3:2513–2517. https://doi.org/10.1021/acssensors.8b01101
18. Qi FP, Zhang Y, Wang BH, Chen WQ, Yang L, Yang ZG, Song XZ (2019) A fluorescent probe for the dicriminatory detecion of Cys/Hcy, GSH and H_2S in living cells and zebrafish. Sens Actuators B 296:126533. https://doi.org/10.1016/j.snb.2019.05.010
19. Yan CX, Shi LM, Guo ZQ, Zhu WH (2019) Molecularly near-infrared fluorescent theranostics for in vivo tracking tumor-specific chemotherapy. Chin Chem Lett 30:1849–1855. https://doi.org/10.1016/j.cclet.2019.08.038
20. Wu P, Xiong H (2022) An acid-enhanced off-on fluorescent probe for the detection of hypochlorous acid in rheumatoid arthritis. Talanta 247:123584. https://doi.org/10.1016/j.talanta.2022.123584
21. Wang WX, Jiang WL, Guo H, Li YF, Li CY (2021) Real-time imaging of alkaline phosphatase activity of diabetes in mice via a near-infrared fluorescent probe. Chem Commun 57:480–483. https://doi.org/10.1039/d0cc07292c
22. Zeng Z, Ouyang J, Sun LH, Zeng C, Zeng F, Wu SZ (2020) Activatable nanocomposite probe for preoperative location and intraoperative navigation for orthotopic hepatic tumor resection via msot and aggregation-induced Near-IR-I/II fluorescence imaging. Anal Chem 92:9257–9264. https://doi.org/10.1021/acs.analchem.0c01596
23. Wu Y, Huang S, Wang J, Sun L, Zeng F, Wu S (2018) Activatable probes for diagnosing and positioning liver injury and metastatic tumors by multispectral optoacoustic tomography. Nat Commun 9:3983. https://doi.org/10.1038/s41467-018-06499-1
24. Zhang K, Zhang J, Xi Z, Li LY, Gu XX, Zhang QZ, Yi L (2017) A new H_2S-specific near-infrared fluorescence-enhanced probe that can visualize the H_2S level in colorectal cancer cells in mice. Chem Sci 8:2776–2781. https://doi.org/10.1039/c6sc05646f
25. Zhou TT, Yang YT, Zhou KY, Jin M, Han MN, Li W, Yin CX (2019) Efficiently mitochondrial targeting fluorescent imaging of H_2S invivo based on a conjugate-lengthened cyanine NIR fluorescent probe. Sens Actuators B 301:127116. https://doi.org/10.1016/j.snb.2019.127116
26. Wu Q, Yin CX, Wen Y, Zhang YB, Huo FJ (2019) An ICT lighten ratiometric and NIR fluorogenic probe to visualize endogenous/exogenous hydrogen sulphide and imaging in mice. Sens Actuators B 288:507–511. https://doi.org/10.1016/j.snb.2019.03.053
27. Tang YW, Li M, Gao X, Liu XY, Gao JW, Ma T, Li JR (2017) A NIR-responsive up-conversion nanoparticle probe of the $NaYF_4$: er,yb type and coated with a molecularly imprinted polymer for fluorometric determination of enrofloxacin. Microchim Acta 184:3469–3475. https://doi.org/10.1007/s00604-017-2387-9
28. Tang LJ, Tian MY, Chen HB, Yan XM, Zhong KL, Bian YJ (2018) An ESIPT-based mitochondria-targeted ratiometric and NIR-emitting fluorescent probe for hydrogen peroxide and its bioimaging in living cells. Dyes Pigm 158:482–489. https://doi.org/10.1016/j.dyepig.2017.12.028
29. Ma T, Huo F, Yin C (2019) A 'naked-eye' ratiometric and NIR fluorescent detection for hydrogen sulphide with quick response and high selectivity for and its bioimaging. Dyes Pigm 165:31–37. https://doi.org/10.1016/j.dyepig.2019.02.001
30. Li S-J et al (2018) Mitochondria-targeted near-infrared fluorescent probe for the detection of carbon monoxide in vivo. Talanta 188:691–700. https://doi.org/10.1016/j.talanta.2018.06.046
31. Keri RS, Patil MR, Patil SA, Budagumpi S (2015) A comprehensive review in current developments of benzothiazole-based molecules in medicinal chemistry. Eur J Med Chem 89:207–251. https://doi.org/10.1016/j.ejmech.2014.10.059
32. Das S et al (2022) Benzothiazole based fluorescent probes for the detection of biomolecules, physiological conditions, and ions responsible for diseases. Dyes Pigm 199:110074. https://doi.org/10.1016/j.dyepig.2021.110074
33. Niu YH, Wang R, Pu L, Zhang YR (2019) Pyrene meets 2-(2-hydroxyphenyl) benzothiazole: creation of highly efficient solid-state monomeric emitter for organic light-emitting diode. Dyes Pigm 170:107594. https://doi.org/10.1016/j.dyepig.2019.107594
34. Taha M, Ismail NH, Imran S, Wadood A, Rahim F, Khan KM, Riaz M (2016) Hybrid benzothiazole analogs as antiurease agent: synthesis and molecular docking studies. Bioorg Chem 66:80–87. https://doi.org/10.1016/j.bioorg.2016.03.010

35. Feng J et al (2023) A fluorescent benzothiazole probe for the detection of carboxylesterase and carbamate pesticides. ChemistrySelect 8. e202303160. https://doi.org/10.1002/slct.202303160
36. Yagai S, Higashi M, Karatsu T, Kitamura A (2006) Tunable interchromophore electronic interaction of a merocyanine dye in hydrogen-bonded supramolecular assemblies scafolded by bismelamine receptors. Chem Commun 14:1500–1502. https://doi.org/10.1039/b516698e
37. Tian T, Hu RR, Tang BZ (2018) Room temperature one-step conversion from elemental sulfur to functional polythioureas through catalyst-free multicomponent polymerizations. J Am Chem Soc 140:6156–6163. https://doi.org/10.1021/jacs.8b02886
38. Mu Y et al (2022) Multiresponsive tetrarylethylene-based fluorescent dye with multicoloreded changes: AIEE properties, acidichromism, Al3 + recognition, and applications. J Mater Chem B 44:9235–9248. https://doi.org/10.1039/D2TB01828D
39. Gopikrishna P, Iyer PK (2016) Monosubstituted dibenzofulvene-based luminogens: aggregation-induced emission enhancement and dual-state emission. J Phys Chem C 120:26556–26568. https://doi.org/10.1021/acs.jpcc.6b09689
40. Chen Z, Liu G, Pu SZ, Liu SH (2017) Carbazole-based aggregation-induced emission (AIE)-active gold (I) complex: persistent room-temperature phosphorescence, reversible mechanochromism and vapochromism characteristics. Dyes Pigm 143:409–415. https://doi.org/10.1016/j.dyepig.2017.05.003
41. Mazumder S, Kumar et al (2022) Synthesis of novel water-soluble chitosan-based off-on fluorescent probes for successive recognitions of Fe^{3+} and F^{-} ions. Iran Polym J 31:425–439. https://doi.org/10.1007/s13726-021-01013-9
42. Li L, Ji YZ, Tang XJ (2014) Quaternary ammonium promoted Ultra selective and sensitive fluorescence detection of fluoride ion in water and living cells. Anal Chem 86:10006–10009. https://doi.org/10.1021/ac503177n
43. Amendola V, Esteban-Gómez D, Fabbrizzi L, Licchelli M (2006) What anions do to N-H-containing receptors. Acc Chem Res 39:343–353. https://doi.org/10.1021/ar0501951
44. Chen S et al (2017) Indolo [3,2-b] carbazole derivative as a fluorescent probe for fluoride ion and carbon dioxide detections. Sens Actuators: B Chem 250:591–600. https://doi.org/10.1016/j.snb.2017.05.012
45. Chen X et al (2017) A highly selective naked-eye and fluorescent probe for fluoride ion based on 1,8-naphalimide and benzothizazole. Dyes Pigm 141:299–305. https://doi.org/10.1016/j.dyepig.2017.02.008
46. Li SJ, Li YF, Liu HW, Zhou DY, Jiang WL, Yang JO, Li CY (2018) A dual-response fluorescent probe for the detection of viscosity and H_2S and its application in studying their cross-talk influence in mitochondria. Anal Chem 90:9418–9425. https://doi.org/10.1021/acs.analchem.8b02068
47. Jin L et al (2019) Modulation of fluorescence sensing properties of coumarin-based fluorescent probe for H_2S and its application in cell imaging. Spectrochim Acta Part A Mol Biomol Spectrosc 221:117187. https://doi.org/10.1016/j.saa.2019.117187
48. Pagidi S, Kalluvettukuzhy NK, Thilagar P (2018) Tunable self-assembly and aggregation-induced emission characteristics of triarylboron-decorated naphthalimides. Organometallics 37:1900–1909. https://doi.org/10.1021/acs.organomet.8b00166
49. Wang BB, Wang QX, Zeng AQ, Leng JC, Zhao W (2021) Engineering a mitochondria-targeted ratiometric fluorescent probe with a large Stokes shift for H_2S-specific assaying in foodstuffs and living cells. Sens Actuators B 343:130095. https://doi.org/10.1016/j.snb.2021.130095
50. Zhang WX, Jia QJ, Meng YY, Chen SJ, Zhang YB, Wang KP, Gan LH, Hu ZQ (2020) Dimethylamino naphthalene-based fluorescent probes for hydrogen sulfide detection and living cell imaging. Spect Acta Part A 228:117835. https://doi.org/10.1016/j.saa.2019.117835
51. Wang BB, Leng JC, Wang XQ, Zhao W (2022) Reversible AIE-active fluorescent probe with a large emission peak shift for ratiometric detection of food freshness indicator H_2S. Food Chem 386:132768. https://doi.org/10.1016/j.foodchem.2022.132768
52. Yi SQ, Liu HL, Chen Z, Fan CB, Liu G, Pu SZ (2023) Novel fluorescent probes based on NBD - substituted imidazole amino to sequentially detect H_2S and Zn^{2+}. Dyes Pigm 214:111211. https://doi.org/10.1039/c6qm00223d
53. Zhang PS, Nie XZ, Gao M, Zeng F, Qin AJ, Wu SZ, Tang BZ (2017) A highly selective fluorescent nanoprobe based on AIE and ESIPT for imaging hydrogen sulfide in live cells and zebrafish. Mater Chem Front 1 5:838–845. https://doi.org/10.1039/c6qm00223d
54. Zhong KL, He YQ, Deng LL, Yan XM, Li XP, Tang YW, Hou SH, Tang LJ (2020) A near-infrared fluorescent probe for H_2S based on tandem reaction to construct iminocoumarin-benzothiazole and its application in food, water, living cells. Anal Chim Acta 1127:49–56. https://doi.org/10.1016/j.aca.2020.06.050
55. Gupta AS, Paul K, Luxami V (2017) A fluorescent probe with AIE + ESIPT characteristics for Cu^{2+} and F^{-} ions estimation. Sens Actuators B 246:653–661. https://doi.org/10.1016/j.snb.2017.02.080
56. He WY, Liu N, Jiang X, Zheng YZ, Lin ZW, Shen JS (2022) Reaction-based fluorescence probes for turn on sensing fluoride ions. Org Biomol Chem 20:1191–1195. https://doi.org/10.1039/d1ob02324a
57. Yang JN, Yuan XW, Wang YL, Liu HL, Pu SZ (2022) A novel turn-on type fluorescent probe with a large red-shift based on TPE for detection of F^{-}. Tetrahedron 129:133167. https://doi.org/10.1016/j.tet.2022.133167
58. Nadimetla DN, Zalmi GA, Bhosale SV (2020) An AIE-active tetraphenylethylene-based cyclic urea as a selective and efficient optical and colorimetric chemosensor for fluoride ions. Chem Select 5:8566–8571. https://doi.org/10.1002/slct.202002126
59. Chen PF, Zhu HC, Kong L, Xu XY, Tian YP, Yang JX (2020) Multifunctional behavior of a novel tetraphenylethylene derivative: mechanochromic luminescence, detection of fluoride ions and trace water in aprotic solvents. Dyes Pigm 172:107832. https://doi.org/10.1016/j.dyepig.2019.107832
60. Iulietto MF, Sechi P, Borgogni E, Cenci-Goga BT (2015) Meat spoilage: a critical review of a neglected alteration due to ropy slime producing bacteria. Ital J Anim Sci 14:4011. https://doi.org/10.4081/ijas.2015.4011
61. Xie L et al (2023) Engineering a mitochondria-targeted fluorescent probe with long wavelength for rapid detection of H_2S in beer, water and living cells. J Photochem Photobiol A 444:114993. https://doi.org/10.1016/j.jphotochem.2023.114993
62. Liu H et al (2023) An off – on NIR fluorescence probe for visualization of H_2S in food spoilage, living cells and zebrafish. Dyes Pigm 209:110888. https://doi.org/10.1016/j.dyepig.2022.110888
63. Yue L et al (2023) A dual-response NIR fluorescent probe for separately and continuously recognizing H_2S and cys with different fluorescence signals and its applications. Analyst 19:4829–4836. https://doi.org/10.1039/d3an00871a